Proc. Natl. Acad. Sci. USA
Vol. 89, pp. 2061–2065, March 1992
Medical Sciences

Three-dimensional structure of Theiler virus

(x-ray crystallography/demyelination/picornavirus/capsid)

ROBERT A. GRANT*†, DAVID J. FILMAN*†, ROBERT S. FUJINAMI‡§, JOSEPH P. ICENOGLE*¶, AND JAMES M. HOGLE*†‖

*Department of Molecular Biology, Research Institute of Scripps Clinic, 10666 North Torrey Pines Road, La Jolla, CA 92037; and ‡Department of Pathology, University of California, San Diego, La Jolla, CA 92093

Communicated by Stephen C. Harrison, December 10, 1991

ABSTRACT **Theiler murine encephalomyelitis virus strains are categorized into two groups, a neurovirulent group that rapidly kills the host, and a demyelinating group that causes a generally nonlethal infection of motor neurons followed by a persistent infection of the white matter with demyelinating lesions similar to those found in multiple sclerosis. The three-dimensional structure of the DA strain, a member of the demyelinating group, has been determined at 2.8 Å resolution. As in other picornaviruses, the icosahedral capsid is formed by the packing of wedge-shaped eight-stranded antiparallel β barrels. The surface of Theiler virus has large star-shaped plateaus at the fivefold axes and broad depressions spanning the twofold axes. Several unusual structural features are clustered near one edge of the depression. These include two finger-like loops projecting from the surface (one formed by residues 78–85 of VP1, and the other formed by residues 56–65 of VP3) and a third loop containing three cysteines (residues 87, 89, and 91 of VP3), which appear to be covalently modified. Most of the sequence differences between the demyelinating and neurovirulent groups that could play a role in determining pathogenesis map to the surface of the star-shaped plateau. The distribution of these sequence differences on the surface of the virion is consistent with models in which the differences in the pathogenesis of the two groups of Theiler viruses are the result of differences in immunological or receptor-mediated recognition processes.**

The Theiler murine encephalomyelitis viruses (TMEVs) are picornaviruses that are most closely related by sequence to the cardioviruses (encephalomyocarditis virus and Mengo virus) (1–3). TMEV strains are classified into two groups on the basis of the disease produced upon intracerebral inoculation of susceptible mice. Members of the GDVII group (the GDVII and FA strains) cause an acute fatal encephalitis associated with lytic infection of motor neurons. Members of the Theiler original (TO) group (including the DA and BeAn strains) are less neurovirulent. They induce a biphasic disease consisting of an early acute poliomyelitis followed by a late, chronic inflammatory demyelinating disease associated with persistent infection of the white matter of the spinal cord. Similarities between TMEV-induced demyelination and multiple sclerosis make the chronic late disease an excellent animal model for an important human disease.

The complete genomes of the DA (3), BeAn (1), and GDVII strains (2) have been cloned and sequenced. Chimeric viruses constructed from these clones (4–8) demonstrate that the 5′ noncoding region of GDVII contains important determinants of neurovirulence (4, 5) and that the ability of DA to persist and demyelinate is determined by a region in the genome that includes capsid protein VP1 (6, 7). Although the central role of VP1 as a determinant of demyelination is disputed (8, 27), its importance also is suggested by the demonstration that two monoclonal escape variants of DA with single amino acid substitutions in VP1 are attenuated in their ability to persist and cause demyelination (9–11). The involvement of capsid proteins in the pathogenesis of the late demyelinating disease implicates the structure of the viral capsid as an important factor in determining the ability of the TO group to persist and cause demyelination and makes these viruses excellent candidates for crystallographic studies of the relationship between structure and viral pathogenesis. We report here the structure of the DA strain of TMEV at 2.8 Å resolution.**

MATERIALS AND METHODS

Virus Production and Crystallization. The DA strain of TMEV (11) was propagated in suspension-adapted BHK cells by modifications of the protocols developed for encephalomyocarditis virus by Rueckert and Pallansch (12), and the resulting virus was purified by differential centrifugation and CsCl density gradient sedimentation (13). Concentrated samples of virus (10 mg/ml) were crystallized at 4°C by microdialysis versus progressively lower concentrations of NaCl in 10 mM Na Pipes buffer (pH 7.0–7.3). The crystals belong to the orthorhombic space group $P2_12_12$ with a = 360.5, b = 338.4, and c = 348.1 Å, and one-half virus particle per asymmetric unit.

Structure Determination and Refinement. X-ray diffraction data were collected at −15°C from randomly oriented crystals by oscillation photography with 0.5° of arc per photograph. The crystals were stabilized by the inclusion of 25% ethylene glycol in the buffer as a cryoprotectant. Photographs were digitized on a 50-μm raster and the reflections were integrated using a recently developed filtering and deconvolution process (D.J.F., unpublished data). Scaling, unit cell, and crystal orientation parameters were refined, and partially recorded measurements were corrected to their fully recorded equivalents as described (14). A final data set, consisting of 1,154,291 measurements of 473,861 unique reflections, was obtained from 38 oscillation photographs of 21 crystals. R_{sym} (for measurements at least 50% observed) was 0.20, where R_{sym} compares multiply measured partiality corrected intensities with their statistically weighted mean.

The publication costs of this article were defrayed in part by page charge payment. This article must therefore be hereby marked "*advertisement*" in accordance with 18 U.S.C. §1734 solely to indicate this fact.

Abbreviations: TMEV, Theiler murine encephalomyelitis virus; TO, Theiler original.

†Present address: Department of Biological Chemistry and Molecular Pharmacology, Harvard Medical School, 240 Longwood Avenue, Boston, MA 02115.
§Present address: Department of Neurology, University of Utah School of Medicine, Salt Lake City, UT 84132.
¶Present address: Division of Viral Disease, Center for Disease Control, Atlanta, GA 30333.
‖To whom reprint requests should be addressed at †.

**The atomic coordinates and structure factors have been deposited in the Protein Data Bank, Chemistry Department, Brookhaven National Laboratory, Upton, NY 11973 (reference 1TME)

The structure of TMEV was determined by molecular replacement, using the atomic coordinates of the closely related Mengo virus (15) as the initial source of phase information. The position and orientation of the particle in the TMEV unit cell were determined early in data processing when only 7% of the unique data to 4 Å were available. Only this small data set was phased directly with the Mengo virus model. Initial phase estimates were refined and extended gradually to higher resolution by repeated application of the phase constraints arising from 30-fold noncrystallographic redundancy (16). As reflections from additional films were processed, they were included in the data set used for phase extension and refinement. Construction of an atomic model was started during phase refinement at 4 Å, when the electron density map unmistakably showed the sequence and conformational differences that distinguish TMEV from Mengo virus. After phases had been extended to include all available data to 2.8 Å resolution, phases based on the atomic model were introduced, and the model and phases were further refined by alternating the application of noncrystallographic symmetry constraints with interactive rebuilding of the model and pseudo-real space refinement (14).

RESULTS AND DISCUSSION

The limited supply of virus made it necessary to collect data from crystals that were relatively small and variable in quality. Consequently, the agreement statistics for the data set are relatively poor (R_{sym} = 0.20), and the reciprocal lattice is sampled incompletely. Nevertheless, the powerful constraints provided by thirtyfold noncrystallographic symmetry resulted in a readily interpretable electron density map (Fig. 1), which correlates well with the predicted amino acid sequence. The averaged Fo map includes well-defined density for residues 1–256 of VP1, 13–266 of VP2, 1–179 and 182–232 of VP3, and 15–39 of VP4. A complete atomic model has been built and refined for these portions of the structure. Statistics for the model are presented in Fig. 2. Residues 257–274 of VP1, 1–12 of VP2, 180–181 of VP3, and 1–14 and 40–71 of VP4 could not be located in the electron density map. Additional electron density features not accounted for by the model are observed on the inner surface of the capsid near the threefold axis. These uninterpretable features may correspond to partially ordered portions of the amino terminus of VP2 or the carboxyl terminus of VP4.

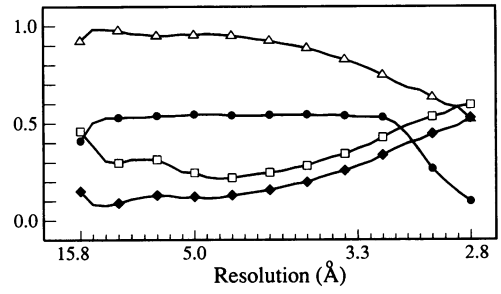

FIG. 2. Agreement statistics for phase refinement are plotted as a function of resolution (Å). ●, Fraction of unique reflections in the shell included in the data set; □, standard crystallographic *R* factor (0.300 overall); △, linear correlation coefficient (0.907 overall); ◆, symmetry-based *R* factor (0.203 overall) assessing the agreement between observed structure factor amplitudes and the Fourier transform of the symmetry-averaged electron density map at convergence. The current atomic model includes 327 solvent atoms with variable individual occupancy factors and 5953 protein atoms. Resolution-dependent bin scales compensate for overall isotropic thermal motion. The model has a 0.04-Å rms deviation of the atomic positions from rigidly constrained groups and a 0.02-Å rms deviation from standard bond lengths.

The DA electron density map contains unusual extra density contiguous with the side chains of cysteines 87, 89, and 91 (Fig. 1) in the exposed CD loop of VP3 (for nomenclature refer to Fig. 3 legend). The sequence in this region has been confirmed, and the extra density persisted in icosahedrally averaged "omit" maps, demonstrating that the extra density is not the result of model-based phase bias. Mengo virus has been reported to contain an unusual and highly strained Cys-Xaa-Cys disulfide bond between the structural equivalents of Cys-87 and Cys-89 (15). The DA electron density maps (Fig. 1) are not consistent with the presence of such a disulfide bond in TMEV. Instead, we interpret the extra density associated with the side chains of cysteines 87, 89, and 91 as evidence for covalent modification. Recently, several biologically relevant cysteinyl modifications (including prenylation, palmitoylation, and methylation) have been described (17). Experiments to confirm and characterize the cysteinyl modifications in DA and to assess their biological relevance remain to be done.

Structure Description. Overall, the architecture of DA is very similar to that of other picornaviruses whose structures have been determined (15, 18–20). Sixty protomers, each

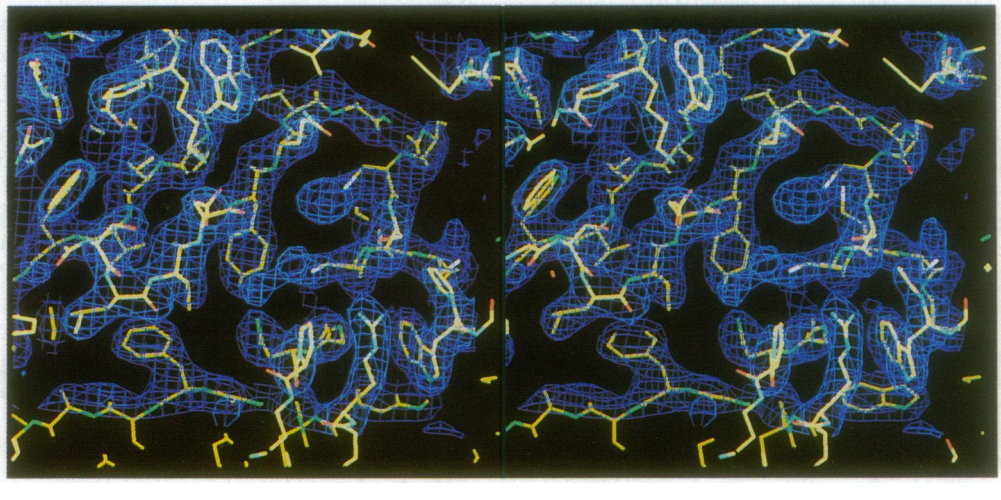

FIG. 1. A portion of the averaged electron density map of the DA strain of TMEV is shown superimposed on the atomic model. In this stereoview, carbons are yellow, oxygens are red, nitrogens are green, and sulfurs are white. Electron density on the left side of the figure, which is readily interpretable, is typical of most of the structure. On the right side of the figure, electron density not accounted for by the model may result from covalent modification of cysteines 87, 89, and 91 of VP3 (see text).

containing three large capsid proteins (VP1, VP2, and VP3) and one small protein (VP4) are arranged to form a $T = 1$ icosahedral shell. The three major capsid proteins have similar wedge-shaped eight-stranded antiparallel β barrel cores that pack to form the continuous protein shell of the virion (Fig. 3). Together with capsid protein VP4, the amino termini of VP1, VP2, and VP3 interact to form an elaborate network on the inner surface of the protein shell. The carboxyl termini of VP1, VP2, and VP3, and most of the loops between β strands are exposed on the outer surface. The outer surface can be represented as the virus-specific decoration of a minimal shell that is formed by packing the wedge-shaped antiparallel β barrel cores of VP1, VP2, and VP3. The minimal shell has broad protrusions at the fivefold axes (where the narrow ends of the VP1 β barrels are clustered), protrusions at the threefold axes (around which the narrow ends of VP2 and VP3 β barrels alternate), broad valleys between these peaks, and saddle-shaped surfaces across the twofold axes. Among the picornaviruses, the largest differences in surface structure correspond to the longest insertions in the loops that connect the strands of the β barrels. In DA [and in Mengo virus (15)], VP1 has relatively large BC and EF loops at the crest of the fivefold peak and a very large double CD loop that broadens the fivefold peak fills much of the valley around it and extends across the valley to form a continuous ridge with the EF loop of VP2. Thus, the surface of the virion is covered by five-pointed star-shaped plateaus whose arms slope gently downward across the surface of VP2 to meet at the threefold axes (Fig. 4*a*). At the crux between each adjacent pair of arms, the star-shaped

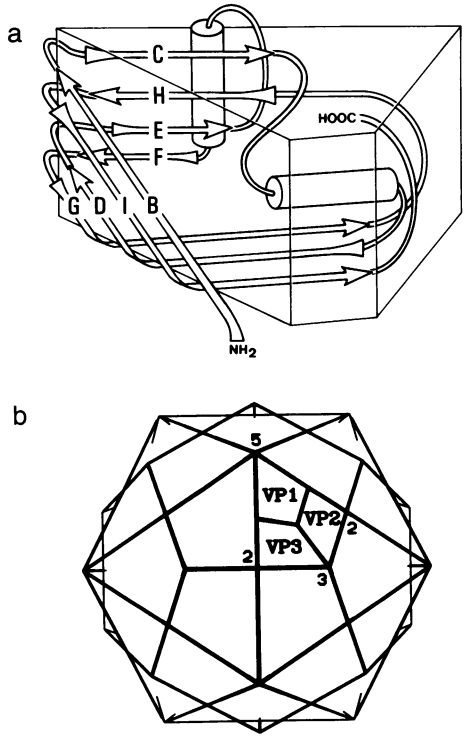

FIG. 3. Structural organization of the major capsid proteins of TMEV. (*a*) Folding pattern of the wedge-shaped eight-stranded antiparallel β barrel core common to the major capsid proteins (VP1, VP2, and VP3) of picornaviruses. By convention, the β strands are designated B–I and the loops are named for the strands they connect. For example, the loop connecting the C and D strands of the β barrel of VP1 is referred to as the CD loop of VP1. (*b*) Locations of the three major capsid proteins from a single protomer are indicated on a simplified geometric representation of the outer surface of the virion. The twofold, threefold, and fivefold symmetry axes adjacent to this protomer are labeled.

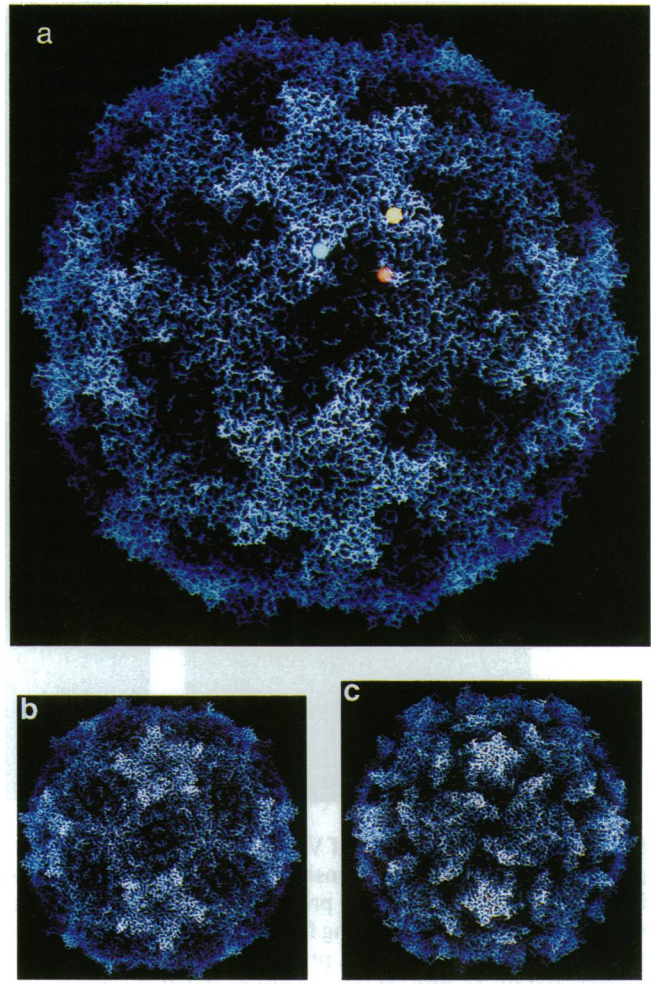

FIG. 4. Appearance of the outer surfaces of three picornaviruses. Atomic models of TMEV (*a*), Mengo virus (*b*), and poliovirus (*c*) are colored in a continuous spectrum from dark blue (low radius) to white (high radius) according to their distance from the center of the virus (radial depth cuing). *a* is shown at twice the scale of *b* and *c*. In *a*, the locations of unusual surface features are marked with colored spheres. The surface features include the VP1 finger (blue sphere), the site of a mutation at VP1 101 that attenuates the ability of DA to persist and demyelinate (yellow sphere), and the modified cysteine residues (residues 87, 89, and 91 of VP3), the VP3 finger, and the carboxyl terminus of VP1 (red sphere).

plateau drops off abruptly into a depression (corresponding primarily to the surface of VP3), which has been called the pit in Mengo virus. The pit area in DA is part of a larger, broad depression that spans the twofold axis. This is also true in the Mengo virus structure (Fig. 4*b*). Indeed, the identification of the pit as a distinct depression in Mengo virus is largely a consequence looking at a roughly spherical surface exclusively in planar sections perpendicular to the twofold axis (15, 21), thereby obscuring the true depth of the surface at the twofold axis.

Surrounding the area corresponding to the Mengo virus pit, there are several unusual and interesting features in the DA structure. These include the modified cysteines and two sets of finger-like projections that stick out into solvent nearly perpendicular to the surface of the virus (Fig. 4*a*). One of these projections, made up of residues 78–85 in the first CD loop of VP1, is located at the edge of the star-shaped plateau, on the rim of the twofold depression. The second projection is an interruption of the B strand of the VP3 β barrel (residues 56–65) and is located near the modified cysteines on the rim of the depression opposite the VP1 finger. Although the

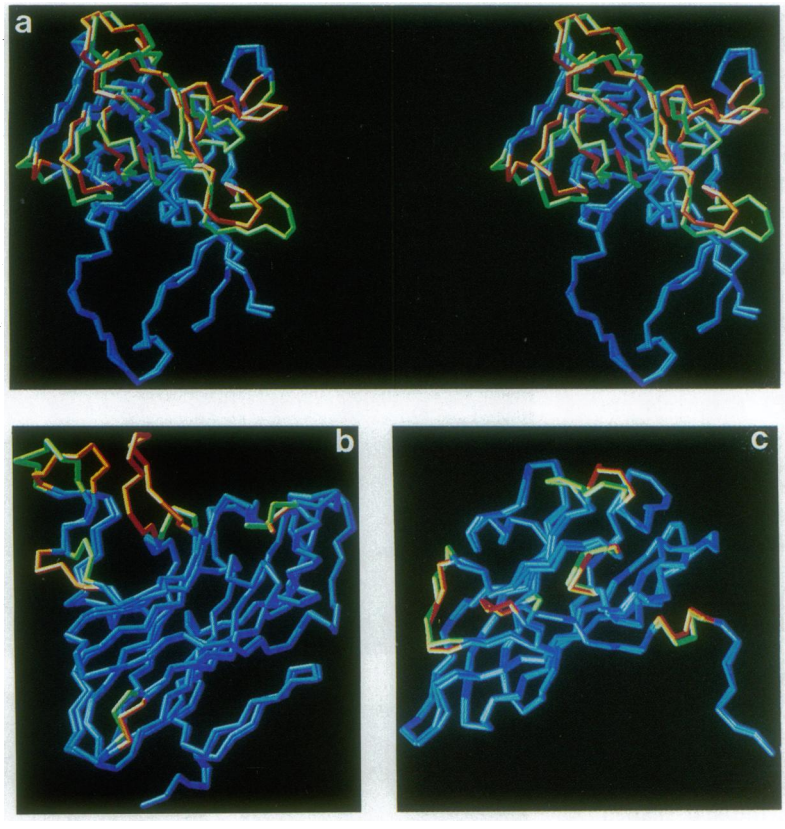

FIG. 5. Similarities and differences in the main-chain conformations of TMEV and Mengo virus are illustrated by superimposed α-carbon models. In *a*, *b*, and *c*, models of VP1 (shown in stereo), VP2, and VP3, respectively, are colored blue in regions where the backbones are most similar. Regions exhibiting the largest differences, generally located on the outer surface of the virion, are highlighted by coloring the TMEV model orange and the Mengo virus model green. In *c*, the amino terminus of VP3, which has a very similar structure in TMEV and Mengo virus, has been truncated for clarity.

interruption in the B strand of VP3 is conserved in all known picornavirus structures, this insertion includes more residues in Theiler virus, and the loop projects more sharply from the surface than the corresponding features in other picornavirus structures. Both finger-like projections can be described approximately as two-stranded antiparallel β-sheets, terminated by β-turns. The β-sheets, however, have disruptions in the hydrogen bonding pattern that are caused by the presence of two prolines in each. Insofar as these unusual projecting hairpin loops play no apparent role in stabilizing the structure of the virus, it is likely that they play a functional role, possibly in immunological or receptor-mediated recognition events.

Comparison with Mengo Virus. Consistent with similarities between their genome and capsid protein sequences, most portions of the DA structure are very similar to the corresponding parts of Mengo virus. However, some portions of the structure, notably loops and carboxyl termini on the outer surface of the virion, have very different conformations (Fig. 5). Particularly dramatic differences occur in the conformations of the double CD loops of VP1 (including the finger-like projection) (Fig. 5*a*), and in the EF loop of VP2 (Fig. 5*b*), corresponding to large differences in the number of amino acid residues in these loops. As these loops all participate in forming the arms of the plateau, the details of the surface structure in this region are markedly different in Mengo virus

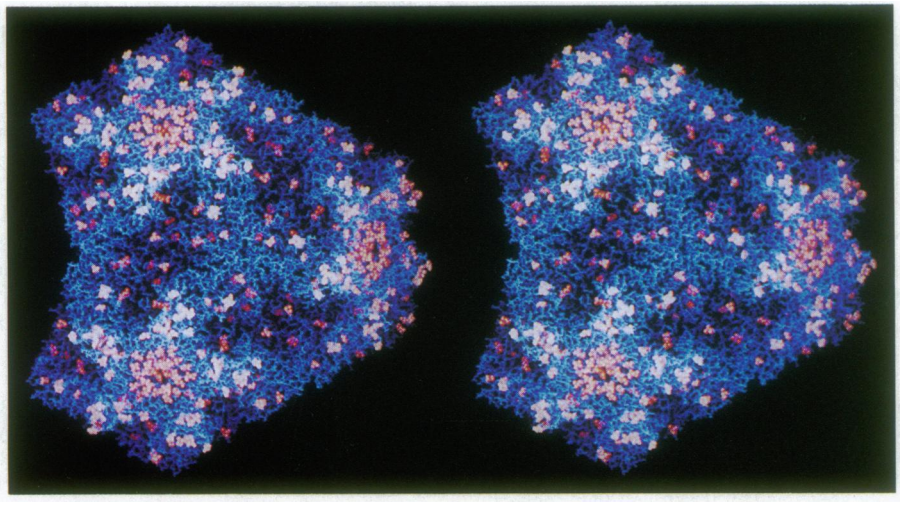

FIG. 6. Sequence differences that distinguish the demyelinating and neurovirulent groups of TMEV are highlighted on an atomic model of the DA strain. In this stereoview, 3 complete pentamers (of 12 in the virion) are depicted with accentuated surface relief. Atoms in the highlighted residues are shown as spheres, in shades ranging from red to white depending on their distance from the center of the virion. These residues are different in the GDVII strain of TMEV from the corresponding residues in both the DA and BeAn strains. While only a small number of these residues are buried beneath the surface of the virion, the overwhelming majority are clustered on the surface of the star-shaped plateau that surrounds the fivefold axis.

and DA (Fig. 4 *a* and *b*). The largest conformational difference in VP3 (Fig. 5*c*) occurs in the finger-like loop that interrupts the B strand of the VP3 β barrel and is related to the greater length of the loop in DA.

The conformational differences cover the star-shaped plateau, including virtually all of the exposed surface of VP1, but are rare over most of the remainder of the surface. This is a particularly striking illustration of the tendency among picornaviruses for the surface of peaks at the threefold axes to be well-conserved and for the surface of the peaks at the fivefold axes to be decorated in a virus-specific way. Virus-specific structures at the fivefold axes may be involved in host-specific recognition events [as is the case for some mouse-adapted strains of poliovirus (14, 22–24)]. Alternatively, structural conservation of the surface at the threefold axes suggests that structural changes in this area may adversely affect viability in some as yet unknown way. In this regard, it is interesting to note that two assembly-defective poliovirus variants with mutations in the BC loop of VP2 (which is located near the threefold axes) have been reported (25, 26).

Relationship Between Structure and Pathogenesis. Interest in the Theiler viruses centers on the different neuropathological properties of the TO and GDVII groups. Comparison of the known TMEV sequences identifies a number of positions where the GDVII strain differs from both the DA and BeAn strains. Although some of these sequence differences may be irrelevant, a subset of them must be responsible for the differences in the pathogenesis of the two groups. The sequence differences in VP1 may be particularly relevant, since recent experiments with chimeric viruses have shown that VP1 contains determinants for persistence and demyelination in DA (6, 7). Most of these residues map into two large clusters exposed on the outer surface of the virion: one in the immediate vicinity of the fivefold axis and the other along the tops of the arms of the star-shaped plateau (Fig. 6). The importance of exposed residues in regulating the course of the disease strongly suggests that recognition (possibly immunological or receptor mediated) may be involved.

Two residues exposed on the surface of the virus, Thr-101 and Val-268 of VP1, have been directly implicated in the chronic demyelinating disease caused by the DA strain of TMEV. For each of these residues, a single-site monoclonal escape mutant of DA has been isolated that has been shown to be attenuated in its ability to persist and cause demyelination (9, 10). These mutants have been shown to cause less severe inflammatory lesions in the spinal cord, and they are cleared efficiently from the nervous system, whereas the wild-type virus persists. In the mutant designated H7A6-2, Thr-101 of wild-type DA is replaced by isoleucine (9). The corresponding residues in BeAn and GDVII are valine and alanine, respectively. Thr-101 is highly exposed at the tip of the second CD loop of VP1 (Figs. 4 and 5*a*) and is located on the rim of the twofold depression. In the second mutant, Val-268 of wild-type DA is replaced by phenylalanine (10). Val-268 is part of the carboxyl terminus of VP1, which is not visible in the electron density map. The last well-ordered residue in the carboxyl terminus of VP1 (residue 256) is located on the exterior surface of the virus adjacent to the VP3 finger. In either of these variants, several mechanisms can be proposed to explain the involvement of exposed residues in the attenuation of demyelination. Attenuation may result from changes that (*i*) make the variants less efficient at infecting specific cells in the spinal cord, (*ii*) cause more efficient clearance of the virus due to alteration of a B- or T-cell epitope, or (*iii*) eliminate an epitope that induces a B- or T-cell response that cross-reacts with a cellular component in myelin-producing cells.

Although the structure at the present time does not provide definitive support for any of the proposed mechanisms of pathogenesis in Theiler viruses, it does suggest that the residues implicated in differences in the pathogenesis of TO versus GDVII-type viruses are likely to be found in a few restricted areas on the exterior surface of the virus. The structure thus provides a framework for the rational design and interpretation of experiments, such as site-directed mutagenesis and the construction of intertypic chimeras, to probe the molecular basis of GDVII neurovirulence and the ability of DA to persist and demyelinate.

We thank Stephan Crainic for assistance in preparing the radial depth cued figures (Figs. 4 and 6); Michael Oldstone, Andrés McCallister, and Michel Brahic for helpful discussions; and Marie Chow for critical review of this manuscript. This work was supported by National Institutes of Health Grant NS12428 (to J.M.H.).

1. Pevear, D. C., Calenoff, M., Rozhon, E. & Lipton, H. L. (1987) *J. Virol.* **61,** 1507–1516.
2. Pevear, D. C., Borkowski, J., Calenoff, M., Oh, C. K., Ostrowski, B. & Lipton, H. L. (1988) *Virology* **165,** 1–12.
3. Ohara, Y., Stein, S., Fu, J., Stillman, L., Klaman, L. & Roos, R. P. (1988) *Virology* **164,** 245–255.
4. Lipton, H. L., Calenoff, M., Bandyopadhyay, P., Miller, S. D., Dal Canto, M. C., Gerety, S. & Jensen, K. (1991) *J. Virol.* **65,** 4370–4377.
5. Fu, J., Stein, S., Rosenstein, L., Bodwell, T., Routbort, M., Semler, B. L. & Roos, R. P. (1990) *Proc. Natl. Acad. Sci. USA* **87,** 4125–4129.
6. McAllister, A., Tangy, F., Aubert, C. & Brahic, M. (1990) *J. Virol.* **64,** 4252–4257.
7. Tangy, F., McAllister, A., Aubert, C. & Brahic, M. (1991) *J. Virol.* **65,** 1616–1618.
8. Fu, J., Rodriguez, M. & Roos, R. P. (1990) *J. Virol.* **64,** 6345–6348.
9. Zurbriggen, A., Hogle, J. M. & Fujinami, R. S. (1989) *J. Exp. Med.* **170,** 2037–2049.
10. Roos, R. P., Stein, S., Routbort, M., Senkowski, A., Bodwell, T. & Wollmann, R. (1989) *J. Virol.* **63,** 4469–4473.
11. Zurbriggen, A. & Fujinami, R. (1989) *J. Virol.* **63,** 1505–1513.
12. Rueckert, R. R. & Pallansch, M. A. (1981) *Methods Enzymol.* **78,** 315–325.
13. Baron, M. & Baltimore, D. (1982) *Cell* **28,** 395–404.
14. Yeates, T. O., Jacobson, D. H., Martin, A., Wychowski, C., Girard, M., Filman, D. J. & Hogle, J. M. (1991) *EMBO J.* **10,** 2331–2341.
15. Luo, M., Vriend, G., Kamer, G., Minor, I., Arnold, E., Rossmann, M. G., Boege, U., Scraba, D. G., Duke, G. M. & Palmenberg, A. C. (1987) *Science* **235,** 182–191.
16. Bricogne, G. (1974) *Acta Crystallogr. Sect. A* **30,** 395–405.
17. Der, C. J. & Cox, A. D. (1991) *Cancer Cells* **3,** 331–340.
18. Hogle, J. M., Chow, M. & Filman, D. J. (1985) *Science* **229,** 1358–1365.
19. Rossmann, M. G., Arnold, E., Erickson, J. W., Frankenberger, E. A., Griffith, J. P., Hecht, H.-J., Johnson, J. E., Kamer, G., Luo, M., Mosser, A. G., Rueckert, R. R., Sherry, B. & Vriend, G. (1985) *Nature (London)* **317,** 145–153.
20. Acharya, R., Fry, E., Stuart, D., Fox, G., Rowlands, D. & Brown, F. (1989) *Nature (London)* **337,** 709–716.
21. Luo, M., Rossmann, M. G. & Palmenberg, A. C. (1988) *Virology* **166,** 503–514.
22. La Monica, N., Kupsky, W. J. & Racaniello, V. R. (1987) *Virology* **161,** 429–437.
23. Martin, A., Wychowski, C., Couderc, T., Crainic, R., Hogle, J. & Girard, M. (1988) *EMBO J.* **7,** 2839–2847.
24. Murray, M. G., Bradley, J., Yang, X.-F., Wimmer, E., Moss, E. G. & Racaniello, V. R. (1988) *Science* **241,** 213–215.
25. Compton, S. R., Nelsen, B. & Kirkegaard, K. (1990) *J. Virol.* **64,** 4067–4075.
26. Reynolds, C., Page, G., Zhou, H. & Chow, M. (1991) *Virology* **184,** 391–396.
27. Rodriguez, M. & Roos, R. P. (1992) *J. Virol.* **66,** 217–225.